

# Investigation of Lead-free Solder Strength on Different Nickel-Phosphorous-plated Nickel's Roughness

Kok-Tee Lau<sup>1,\*</sup>, Cheng-Guan Ong<sup>2</sup>, M. Zaimi<sup>3</sup>

<sup>1</sup>Faculty of Engineering Technology, Universiti Teknikal Malaysia Melaka, 76100 Durian Tunggal, Melaka, Malaysia.

<sup>2</sup>Infineon Technologies (Malaysia) Sdn Bhd, Free Trade Zone, Batu Berendam, Melaka, Malaysia.

<sup>3</sup>Faculty of Manufacturing Engineering, Universiti Teknikal Malaysia Melaka, 76100 Durian Tunggal, Melaka, Malaysia.

(\*Corresponding author)

## Abstract

Thin Small Leadless Packages (TSLP) have been manufactured to cater to current industry demand for a smaller electronic apparatus with higher electrical performance. The current study investigated the effect of TSLP's pad surface roughness ( $R_a$ ) on the solder joint strength of TSLP as functions of etching factors (i.e. Cu alloy leadframe grade, conveyor speed,  $\text{CuCl}_2$  etchant's pH and specific density) and its corresponding failure mode after a shear test. Consequently, the study also looked at the effect of Ni-P plating thickness as well as solder reflow conditions (i.e. temperature and duration). The solder joint of Ni-P plated TSLP's pad exhibited shear strength increase and a reduction in strength variation with the decrease of Ni-P's  $R_a$  at larger thicknesses. Higher  $R_a$  samples exhibited greater strength than the low  $R_a$  samples after reflow due to lower solder porosity of the former. The majority of failure modes happened at the solder due to the formation of a fracture at the high-stress porous solder region. Failure at IMC was eliminated when the pad's  $R_a$  decreased. It was clearly shown that solder joint strength, its variance and the failure mode of TSLP were influenced by the pad and Ni-P's roughness.

**Keywords:** Chemical Etching, Coatings, Electroless Nickel Immersion Gold (ENIG), Shear Strength, Surface Roughness

## INTRODUCTION

In recent years, there has been increased interest in the manufacturing of Thin Small Leadless Packages (TSLP) for high frequency application (e.g. in mobile systems) [1]-[6]. The TSLP is similar to the Quad Flat No-Lead (QFN) package in terms of leadless design, but is thinner, with less parasitic capacitance effect [1]. It has been manufactured to cater to current industry demand for a smaller electronic apparatus with higher electrical performance. TSLP has very small and thin integrated contact areas as second level interconnects [7]. The leadless package design helps to improve the manufacturing process and its thermal management aspect, besides reducing pad/solder interfacial stresses [7], [8].

Along with this growth in TSLP demand, semiconductor manufacturers are constantly striving to increase the performance of TSLP while decreasing its cost of manufacture. The cost reduction could be achieved through better assembly technology and the utilization of low-cost materials. Currently, Infineon Technologies is exploring the

usage of EFTECH-64 grade copper (Cu) alloy as an alternative TSLP leadframe material to the well-known C194 grade alloy. The Cu alloy leadframe is essential for making Ni pad arrays that subsequently serve as the interconnects of TSLPs. During the assembly process, the leadframe acts as temporary structural support for the Ni pads for the subsequent die attach, die-to-package interconnection and mold encapsulation processes [7]. Consequently, the whole Cu alloy leadframe is etched away, revealing all the bottom part of the Ni pads embedded in the mold package. The exposed pads become the pads of the TSLP. For surface finish, electroless nickel immersion gold (ENIG) plating is performed on the pads to improve solderability, corrosion resistance and mechanical strength [9], [10]. The oxidation resistant immersion gold (IG) layer is very thin. Hence, it is normally destroyed during the soldering process [11].

Despite its well-established plating process, obtaining a high solder joint (viz. shear) strength for electroless nickel (EN) plating for different pad surface roughnesses remains a challenge and requires careful process optimization [12]. Although the effect of different substrate materials on the EN plating is well established [13], the studies on the surface roughness of depositing substrate on the EN plating properties are limited to a number of substrate materials [14]. In one investigation into EN plating on glass fiber-reinforced plastic, it was found that EN plating on a substrate with high surface roughness exhibited higher micro-hardness and corrosion resistance [15]. Another study by Liu and Gao [16] showed that the rough Mg alloy substrate contributed to a more uniform microstructure, with thicker and higher adhesion EN plating. The phenomenon is explained by Sahoo and Das [14] who suggest that the surface roughening of substrate prior to the EN plating resulted in more active sites that are favourable for EN plating. They proposed that the increase of active sites results in more hypophosphite adsorption, a process that enables subsequent nickel precipitations and phosphorous co-depositions [14]. In view of all that has been mentioned so far, one may suppose that TSLP contact roughness plays a vital role in the shear strength of ENIG plating. For solder-joint performance of TSLP in the package-to- printed circuit board (PCB) interconnection to be improved, pad surface roughness need to be optimized.

There is an unambiguous relationship between pad surface roughness with the wet etching process of TSLP's Cu alloy leadframe because of the direct physical contact of the leadframe with the pad's bottom [7]. The wet etching

mechanism involves the oxidation of metal by oxidizing agents followed by the formation of metal-ligand complexes to remove the oxidized metal from the surface [17]. At Infineon Technologies, wet etching has been performed using cupric chloride ( $\text{CuCl}_2$ ). The etching solution is widely used in the electronics industry because of its easy regeneration capability, highly reproducibility and low waste production [18], [19]. Several detailed studies have been conducted on the effect of  $\text{CuCl}_2$  wet etching on the surface roughness of copper and copper alloy specimens [18], [20]-[22]. One of the studies found that high purity copper's surface roughness ( $R_a$ ) increased when the etching rate increased [21]. A positive correlation between  $R_a$  and the etching rate was also displayed by the etching of single crystal silicon using other etchants at increasing concentrations [23], [24]. Another study on a Cu-Zn alloy (i.e. CZ108 brass) showed that its  $R_a$  decreased with a higher etching temperature (i.e. at 20-50°C range), depth of etch (i.e. at 50-135  $\mu\text{m}$  range) and  $\text{CuCl}_2$  concentration [20]. We expect different copper alloy leadframes to exhibit different  $\text{CuCl}_2$  etching rates because of the different nobilities exhibited by the different Cu alloys [25]. Consequently, the etching of different Cu alloy leadframe (i.e. in contact with the TSLP's pad) may produce different pad roughness. Thus, the Cu alloy leadframe material is considered to be one of the important factors affecting the solder joint strength of TSLP.

Since European environmental protection agencies (i.e. WEEE and RoSH) imposed the lead-free solder materials requirement in electronic appliances in 2006, different lead-free solder materials have been used by semiconductor manufacturers to replace tin-lead solders [26]. It was claimed that tin-silver (Sn-Ag) alloys are strong candidates among the lead-free alloy alternatives, since their properties are reasonably compatible with those of the tin-lead solder alloy [26]. Other commercially available lead-free solders are tin-silver-copper (SAC) alloys which have been widely reported in the literature [26], [27]. Reflow temperature and thermal reliability studies on the solder joint strength of EN plating with Sn-Ag solders have been investigated through the cross-sectional examination of the formed intermetallic compounds (IMC) [9], [28]. The studies show the presence of three layers of intermetallic compounds (IMC):  $\text{Ni}_3\text{Sn}_4$ , Ni-Sn-P, and  $\text{Ni}_3\text{P}$  between the Sn-3.5 Ag solder and EN layer (i.e. Ni-P) right after reflow. The IMC layers continued to grow thicker with increasing thermal aging duration at the expense of Ni-P layer thickness [9], [28]. Similarly, IMC growth from the SAC solder and Ni-P interface also consumed the Ni-P layer as the solder joints were exposed to a longer thermal duration [11], [29]. Overall, these studies showed that the IMC formation is influenced by the EN plating properties, which then had a significant impact on the solder joint strength and failure mode of the soldered ENIG plated TSLP's pad.

The current paper reports on the effect of the TSLP pad's surface roughness on solder joint (shear) strength on the PCB after the ENIG plating, and flux soldering processes. Four factors that predominantly affect the pad's surface roughness were investigated in terms of their correlation behaviors. These factors are leadframe materials, etching time (i.e.

controlled by the conveyor speed of etching equipment), pH and specific Cu density of  $\text{CuCl}_2$  etchants (i.e. related to etchant concentration). The final part of the paper relates the Ni-P thickness and solder reflow conditions (i.e. temperature and duration) of the TSLP's pad on the solder joint strength and the corresponding failure modes.

## MATERIALS AND METHODS

Firstly, Ni pads were formed onto a copper alloy leadframe as per the required patterns. Two types of leadframes were used, namely EFTECH-64- and C194-grade copper alloys (their chemical compositions are shown in Table I). Both the leadframes had a thickness of 12  $\mu\text{m}$ . The leadframes acted as temporary structural support for the Ni pads in TSLP assembly process. After completing the die attach, the first level interconnection (i.e. wire bonding or flip clip process) and the mold encapsulation processes, the leadframes were etched away using a  $\text{CuCl}_2$  etchant (Macdermid) in a chemical etching machine (brand: PILL). The equipment had a conveyor belt set-up to control spray etching exposure time, and a chemical bath setting to control the specific Cu gravity (i.e. corresponding to  $\text{CuCl}_2$  concentration) and the pH of  $\text{CuCl}_2$  etchant solution. The pH of the etchant was controlled by the amount of ammonium chloride ( $\text{NH}_4\text{Cl}$ ) addition.  $\text{NH}_4\text{Cl}$  was added to improve the etching properties [22]. After the backsides of Ni pads in the TSLP mold package were revealed, the pads' surfaces were cleaned using hydrochloric acid and distilled water at room temperature. The etched samples were categorized into two sample groups and were named as EFTECH-64 and C194 samples. The names were based on the grade of leadframe supporting the Ni pads before underwent leadframe etching process.

**Table 1.** Comparison of Chemical Compositions of EFTECH64 and C194 Copper Alloys

Elements (in wt%)	Copper Alloy Grade	
	C194 [30]	EFTECH-64 [31]
Sn	-	0.23-0.27
Cr	-	0.20-0.30
Zn	0.13	0.18-0.26
Fe	2.35	-
P	0.08	-
Cu	97.44	99.17-99.39

The full factorial design of experiment (DOE) analysis of the etched was performed using the CEDAS software. Details of the levels of the input factors (etching parameters) are tabulated in Table 2. The conveyor speed, specific Cu gravity and pH of the etchants were selected to achieve the pad's

average surface roughness ( $R_a$ ) target of  $0.11 \mu\text{m}$  with six-sigma error range [32]. DOE analysis involved  $54 (=2^1 \times 3^3)$  runs or samples. After that, surface roughness measurements (i.e. output response) were carried out on these samples by Hommel Tester 1000T apparatus. Ten measurements were obtained for each sample to obtain the average value. The measured  $R_a$  value (i.e. arithmetic average value within the measuring length) was conducted in one straight line based on IPC standard IPC-TM-650 (no. 2.2.17A) [33].

**Table 2.** Levels of the  $\text{CuCl}_2$  Etching Factors used in the DOE Analysis

Factor (unit)	Level		
	1	2	3
Cu alloy Leadframe Grade	C194	EFTECH-64	-
Conveyor Speed (m/min)	10	20	30
pH	8.0	8.5	9.0
Specific Cu density ( $\text{g}/\text{cm}^3$ )	1.210	1.220	1.230

Next, EN plating was performed on the etched samples using commercial electroless nickel solution at  $84 \pm 5^\circ\text{C}$  to obtain Ni-P layers with thickness of 0.5, 2.5 and  $4.5 \mu\text{m}$ . Then, IG plating was applied onto the Ni-P to form  $\sim 0.08 \mu\text{m}$  thick Au layer for oxidation resistance. The ENIG plating used the etched EFTECH-64 and C194 samples prepared at optimized etching factors:  $\text{CuCl}_2$  specific gravity of 1.225, pH of 8.4 and conveyor speed of 15-25 m/min. For the adhesion and shear test, the conveyor speed was fixed at 22 m/min (i.e. at midpoint of 20 and 25m/min) to obtain pad's  $R_a$  target of  $0.11 \pm 3 \mu\text{m}$  [32]. The ENIG's thickness (i.e. average value of 10 measurements) and surface roughness were conducted using the Hommel Tester 1000T apparatus according to the IPC standard IPC-4552 [34] and IPC-TM-650 (no. 2.2.17A) [33] respectively.

Characterization of adhesion strength of the pads' Ni-P plating was conducted using 850D Adwill Tape 3M equipment as per IPC standard TM-650 No. 2.4.1 [35]. Firstly, the D850 adhesive tape was applied on the pads' surface of TSLP package array (i.e. consisted of few hundred to few thousand molded units). After the package array was fixed, the tape was peeled from one side at a peeling rate of 0.2 cm/s. The surfaces of the tape and TSLPs' pads were inspected for the Ni-P/Au plating remains. The test samples passed the adhesion test when no Ni-P/Au plating remains were detected on the peeled adhesive tape.

The TSLP package's shear test was performed at room temperature to assess the solder joint strength of the TSLP package after PCB mounting. After solder dispensing with Sn-3.5 wt% Ag solder ball, the TSLP package was placed on the

PCB at the pads. Then, the settings underwent reflow in a nitrogen environment at different reflow temperatures and durations to complete the solder processes. The reflow profile was in accordance with JEDEC J-STD-020D standard [36]. The shear test was conducted on fifty (50) randomly selected samples using a Bond Tester (Model: Dage Series 4000, 500 g test load). The shear height and test speed of the package shear work were  $135 \mu\text{m}$  and  $400 \mu\text{m}/\text{s}$ .

Microstructural examinations were conducted by scanning electron microscopy (SEM, 5 and 15 kV accelerating voltage, JEOL JSM-6360A) on the TSLP pad's surface right before and after the ENIG plating, as well as after the adhesion test and shear test. Energy dispersive X-ray (EDX) was used to characterize the Ni-P and IMC composition, as well as identify the failure mode of the shear test samples.

## RESULT AND DISCUSSION

### Etched TSLP's Pad

Figure 1 shows that Cu alloy leadframe grade has the most significant influence on the reduction of the pad's surface roughness. A change of leadframe from C194 to EFTECH-64 caused a huge drop in the pad's surface roughness ( $R_a$ ) at different conveyor speeds, pH and Cu specific densities. The leadframe grade factor caused the largest  $R_a$  change (i.e. 36% difference between the C194 and EFTECH-64 samples) as compared to the conveyor speed, pH and Cu specific density factors. An average difference of 26% of  $R_a$  was measured when the conveyor speed, pH and Cu specific density factors changed from a low to high level (indicated by blue and green lines respectively in the Figure 1). For both leadframe grades, the  $R_a$  decreased when a higher conveyor speed, lower pH and higher Cu specific density were selected. The interactions between the four factors were insignificant in the studied range as no plot crossing was observed (see Figure 1).

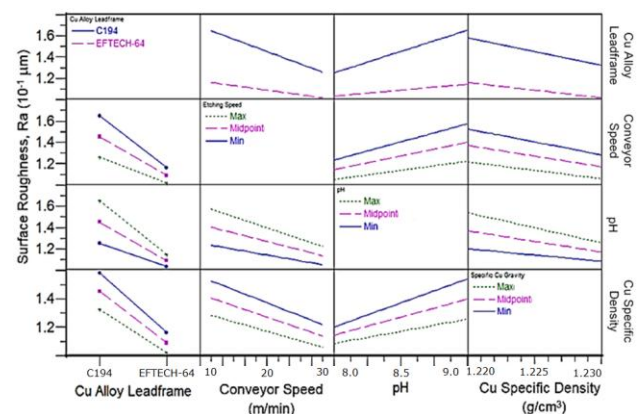


**Figure 1.** Interaction plots for surface roughness

Figure 2 shows that the ridges on the surface of the etched C194 sample are deeper and wider than the etched EFTECH-64 sample. However, the ridges became less apparent (i.e.

ridge's depth decreased) with the increasing conveyor speed. Obviously, samples with deeper ridge microstructures corresponded to higher  $R_a$ . The ridges in the EFTECH-64 appeared more aligned in parallel than in the C194 although were less depth.

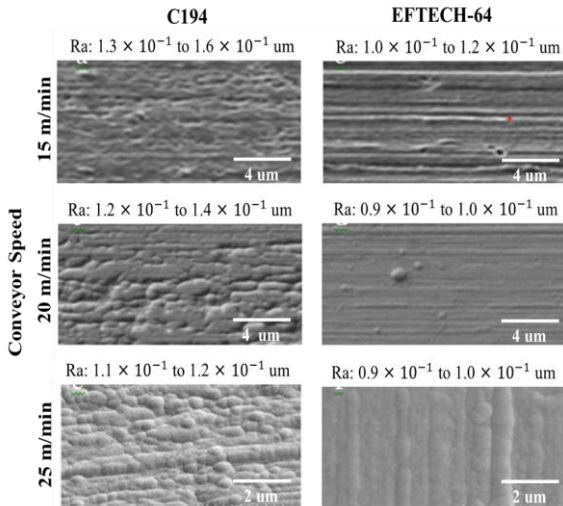


**Figure 2.** Surface microstructure of Ni pad after etching of leadframe taken by SEM at 5 kV accelerating voltage

The  $\text{CuCl}_2$  spray etching process involved sprinkling the  $\text{CuCl}_2$  etchant onto the etched specimen [37]. Since the conveyor belt ran in a single direction, parallel line microstructures (i.e. ridges) were formed on the etched metal surface immediately after etchant spray mist reacted on the leadframe surface. The remnant of the parallel ridges was exhibited on the Ni pad surface (illustrated in Figure 2) when the overlaid leadframe was completely etched.

Spray etching of C194 and EFTECH-64 leadframes overlaying the TSLP produced lower pad's  $R_a$  in the latter because of a slower etching rate of the latter alloy. Table I indicated the EFTECH-64 alloy was containing less electropositive Cr and Sn alloying elements as compared to Fe and P in the C194 alloy [38]. The low etching rate enabled a more uniform chemical removal of metallic ion from the EFTECH-64 surface, resulting in a low  $R_a$ .

A higher conveyor speed means shorter etching time of the etched specimen [37]. A shorter spray mist exposure time reduced the amount of etchant that landed on the leadframe surface. This reduced the etching rate, resulting in a lower  $R_a$ .

Higher Cu specific density indicates higher  $\text{CuCl}_2$  concentration [39]. A higher Cu specific density etchant produced lower  $R_a$ , because of a lower etching rate [20]. The low etching rate was attributed to the increase of etchant viscosity which increased higher  $\text{CuCl}_2$  concentration [20].

The pH of the  $\text{CuCl}_2$  etchant correlated with the amount of ammonium chloride ( $\text{NH}_4\text{Cl}$ ) added. Previous studies reported

that the addition of  $\text{NH}_4\text{Cl}$  accelerated the  $\text{CuCl}_2$  etching process [18], [22]. Thus, a higher etching rate explained the observed higher  $R_a$  for higher pH value (i.e. corresponding to more  $\text{NH}_4\text{Cl}$  addition).

Contour plots (as shown in a previous paper) derived in Fig. 1 showed that the EFTECH-64 etching produced lower pad's  $R_a$  variation than the C194 samples at a  $\text{CuCl}_2$  specific gravity of  $1.225 \text{ g/cm}^3$  within the studied conveyor speeds (i.e. 10-30 m/min) and pH (i.e. 8.0-9.0) ranges [32].  $R_a$  of EFTECH-64 and C194 samples varied within the 0.1-0.125  $\mu\text{m}$  and 0.11-0.19  $\mu\text{m}$  ranges respectively. The  $R_a$  of the etched samples was predominantly affected by TSLP pad location relatively to the  $\text{CuCl}_2$  spray direction. Since etching of TLSP packages were performed in arrays on a moving conveyor by fixed position  $\text{CuCl}_2$  spray heads, some of the TSLP's pads would have been exposed to different amounts of  $\text{CuCl}_2$  etchant. However, C194 samples had significantly higher etching rate than the EFTECH samples. Thus, the former produced a comparatively higher  $R_a$  variance than the latter samples at the same etching parameters.

### ENIG Plated TSLP's Pad (Prior to Flux Soldering)

Figure 3 shows etched C194 samples with different  $R_a$  at before and after 2.5  $\mu\text{m}$  thick ENIG plating. The etched microstructure was slightly altered after ENIG plating where the  $R_a$  of the plated samples was slightly lower than the etched samples. The  $R_a$  results confirmed the previous findings on the correlation of ENIG plating  $R_a$  on the etched substrate's  $R_a$  [14], [15].

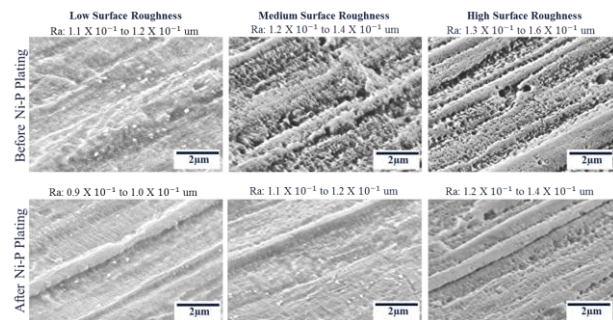


**Figure 3.** Surface microstructural comparison of the C194 samples before and after 2.5  $\mu\text{m}$  thick Ni-P plating. The different etched surface roughness were prepared using different conveyor speeds

All the plated EFTECH-64 and C194 samples exhibited smooth cross-sectional Ni-P microstructure and P content (i.e. 8 wt%), regardless of the Ni-P thicknesses (i.e. 0.5, 2.5 and 4.5  $\mu\text{m}$ ) [12]. This suggests that all samples had a similar Ni-P nodule microstructure although they had different etched  $R_a$ . Previous studies showed a correlation of Ni-P nodule size with P content [15].

Nevertheless, C194 sample plated at 0.5  $\mu\text{m}$  Ni-P thickness demonstrated peeled fracture at the pad/Ni-P interface after the adhesion test (Fig. 4). However, the C194 sample passed the adhesion test when thicker Ni-P thicknesses (i.e. 2.5 or 4.5  $\mu\text{m}$ ) were plated. It is speculated that the substandard adhesion strength of the 0.5  $\mu\text{m}$  Ni-P was caused by below par Ni-P nodule strength near the pad interface. After a prolonged (and thicker) Ni-P plating, the Ni-P nodule microstructure was strengthened.

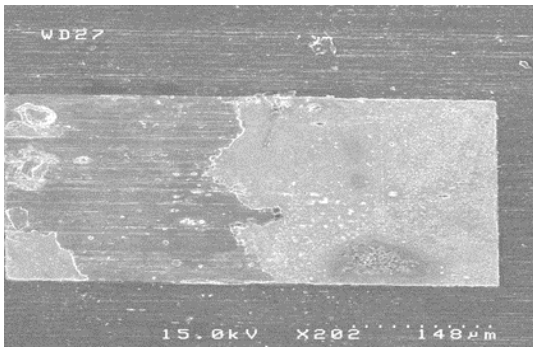


**Figure 4.** SEM surface image of 0.5  $\mu\text{m}$  Ni-P plated on C194 sample's pad after adhesion test

#### Soldered ENIG Plated TSLP's Pad (After Reflow)

Figure 5 showed that shear strength behavior of Sn-Ag soldered ENIG samples versus Ni-P thickness depended on the TSLP's leadframe grade. Since the etched C194 and EFTECH-64 samples had significantly different  $R_a$ , their  $R_a$  should have influenced the shear strength values. Furthermore, a larger shear strength variation seems to correlate with a higher sample's  $R_a$ . For instance, the  $R_a$  for the EFTECH-64 samples was smaller than the C194 samples, which correlates with smaller strength variation in EFTECH-64 as compared to the C194.

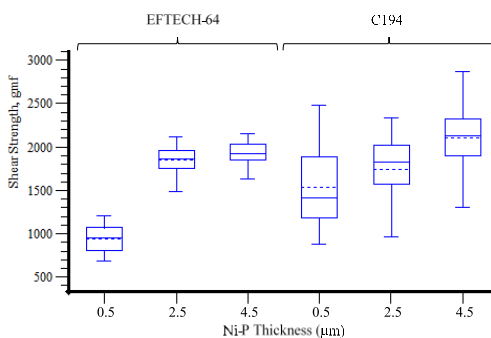


**Figure 5.** Box plot of shear strength of solder jointed EFTECH-64 and C194 samples plated with different Ni-P thicknesses. Reflow temperature and duration were set at 260°C for 1 min.  $R_a$  of EFTECH-64 and C194 samples prior to ENIG plating were measured at  $0.110 \pm 0.015 \mu\text{m}$  and  $0.1395 \pm 0.0525 \mu\text{m}$  respectively, etched using optimum etching parameters.

For C194 samples, shear strength increased proportionally with Ni-P thickness. However, a similar Ni-P thickness increase of the EFTECH-64 contributed to a logarithmic increase of the shear strength. Since  $R_a$  decreased after Ni-P plating (as exhibited by the Figure. 3), the strength increase trend and the strength robustness (i.e. low strength variation) may be connected to the decrease of the  $R_a$  of the plated samples. The EFTECH-64 samples had low etched  $R_a$  (i.e. 0.09-0.1  $\mu\text{m}$ ). So, the samples started to show insignificant  $R_a$  reduction after Ni-P plating thickness increased from 2.5 to 4.5  $\mu\text{m}$ . This explained how the strength plateaued at a Ni-P thickness of 2.5  $\mu\text{m}$ . On the contrary, the C194 samples because of their relatively higher etched  $R_a$ , continue to show significant  $R_a$  reduction after thick Ni-P plating. Thus, the corresponding strength increased linearly from 0.5 to 4.5  $\mu\text{m}$  Ni-P thickness.

Meanwhile, both sample groups achieved smaller strength variations when coated with a larger Ni-P thickness. This was particularly obvious for C194 where a significantly reduced strength variation was observed when Ni-P thickness increased from 0.5 to 2.5  $\mu\text{m}$ . It appears that the increase of Ni-P thickness reduced the  $R_a$  of the C194 and EFTECH-64 samples, and this may contribute to a smaller variation of etched  $R_a$ . It is suspected that a larger  $R_a$  variation of C194 than the EFTECH-64 before plating (as shown in Figure 2) was also been exhibited after thin Ni-P plating. Consequently, C194 strength displayed large and non-normal strength distribution (i.e. mean not equal to median values) at low Ni-P plating thickness of 0.5 and 2.5  $\mu\text{m}$ . For instance, the strength histograms of the 0.5  $\mu\text{m}$  Ni-P plated samples (in the Figure 6) showed C194 displaying two broad distributions, as compared to a narrow distribution for the EFTECH-64. The above observation further supported the earlier argument that the sample's  $R_a$  (i.e. either from the ENIG plated or etched surface) played a dominant role in the determination of shear strength of the soldered samples.

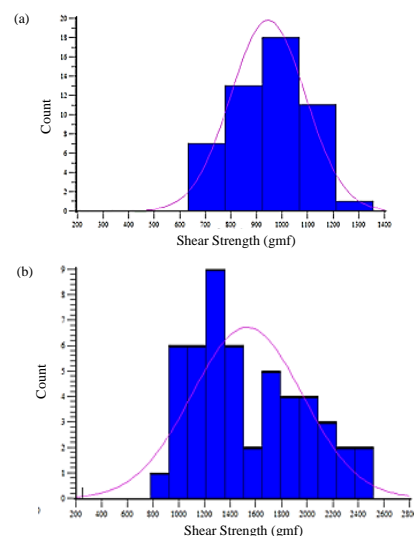


**Figure 6.** Shear strength histogram distribution of soldered 0.5  $\mu\text{m}$  Ni-P plated EFTECH-64 (a) and C194 (b) samples. Reflow temperature and duration were set at 260°C for 1 min

### Failure Mode Analysis

Failure mode analyses were performed by SEM-EDX technique on the PCB fracture side of the samples' contact pads. The failure modes were differentiated in terms of the location of crack propagation. Modes 2 and 3 occurred along the Ni/Ni-P and Ni-P/IMC interfaces respectively, whereas Mode 1 propagated solely in the solder region (illustrated in Figure 7). In the case when there were more than one failure modes appearing on the same sample, the dominant failure mode was assigned as the failure mode of the sample. It is supposed that the existence of multiple failure modes on the same samples was caused by the  $R_a$  variance on the same contact pad of the etched sample, which then affected the solder joint of the Ni-P plated samples.

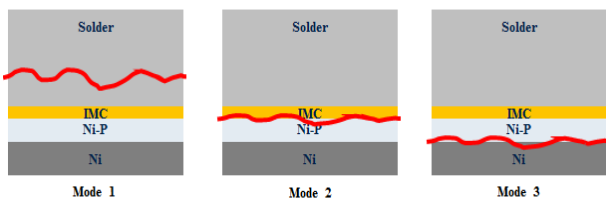


**Figure 7.** Schematic illustrations of the three failure modes occurred in the shear test samples. (red line: fracture path)

Figure 8 shows failure mode distribution of shear test samples (i.e. underwent reflow at 260°C for 1 min). Most of these shear samples displayed Mode 1 failure that included all the EFTECH-64 samples. Only 4% of the C194 samples with Ni-P thickness of 0.5 μm exhibited Mode 2 failure. The absence of Mode 3 failure in the reflowed and soldered 0.5 μm Ni-P plated C194 samples indicates the significant increase of Ni-P plating adhesion strength on the Ni pad as compared to samples before reflow (as shown by sample of Figure 4). The presence of Mode 1 and 2 failures in the 0.5 μm Ni-P plated C194 samples may result in a large strength variation (see Figure 5 and 6). It seems like the occurrence of Mode 2 failure on the soldered 0.5 μm Ni-P plated C194 samples did not correlate with its shear strength because the C194 samples' shear strengths were still comparatively higher than the 0.5 μm Ni-P plated EFTECH-64 samples. The strength data was determined quantitatively through shear test. Whereas, failure mode analysis involved qualitative fracture identification in which dominant failure mode on the samples were identified.

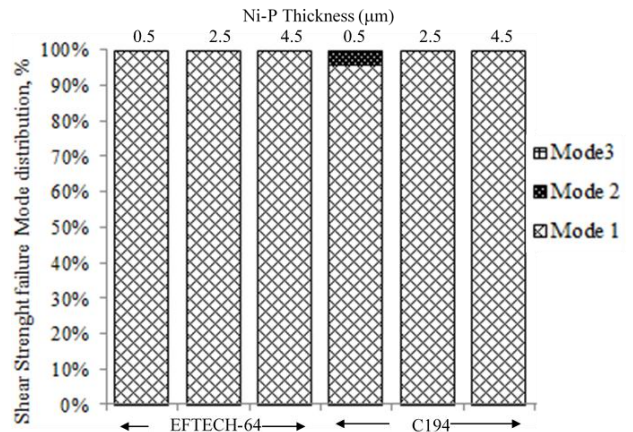


**Figure 8.** Failure mode distribution of shear test samples by leadframe grade and Ni-P thickness. Reflow temperature and duration were set at 260°C for 1 min

Nearly all of the shear failures happened in the form of Mode 1, in which the crack might propagate along the porous Sn-Ag solder, as illustrated in our previous paper [12]. It is presumed that shear strengths of the related soldered samples was predominantly determined by the porosity of the Sn-Ag solder. However, the solders' porous microstructure did not exhibit correlations with the leadframe grade and Ni-P thickness on the observed samples. The observation was consistent with the large shear strength variation for these samples (see Figure 5).

Our earlier discussion stated that  $R_a$  of Ni-P plated C194 was comparatively higher than the Ni-P plated EFTECH-64 samples, and their  $R_a$  decreased with the increase of Ni-P plating thickness. It was claimed by other studies that a higher  $R_a$  resulted in a lower solder wettability on the Ni-P [40], [41]. The higher percentages of Mode 2 and 3 failures (i.e. failure at IMC interface) on the C194 than the EFTECH-64 samples (see Figure 8) may be due to the reduced solder wettability caused by a higher  $R_a$  of the former.

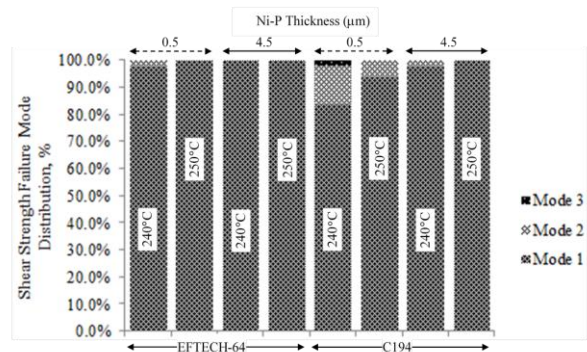


**Figure 9.** Failure mode distribution of shear test samples by leadframe grade, reflow temperature and Ni-P thickness. Reflow duration was set at 10 min

Figure 9 shows that the failure mode distribution of shear samples reflowed at a longer reflow duration (i.e. 10 min) versus leadframe grade and lower reflow temperatures. C194

shear samples exhibited a larger change in terms of failure mode distribution as compared to EFTECH-64 samples as the reflow conditions varied. Reflow at lower temperatures and extended reflow duration triggered higher percentages of Mode 2 and 3 failures in the 0.5  $\mu\text{m}$  Ni-P plated C194 samples. For instance, 0.5  $\mu\text{m}$  Ni-P plated C194 samples reflowed at 240°C and 10 min exhibited 14% and 2 % for Mode 2 and 3 respectively, as compared to 4 % and 0 % for the same modes when reflowed at 260°C and 1 min (i.e. Figure 8). The new reflow conditions also triggered formation of Mode 2 failure in 4.5  $\mu\text{m}$  Ni-P plated C194 and 0.5  $\mu\text{m}$  Ni-P plated EFTECH-64 samples.

Previous studies showed that IMCs' thicknesses and void formation (i.e. in Ni<sub>3</sub>P and Ni-Sn compounds) increased at a higher reflow temperature and longer reflow duration [9], [29]. A comparison of Figure 8 and 9 data showed that reflow duration was affected more significantly than reflow

temperature to the failure modes. For instance, in C194, the change of failure mode occurrence's percentage was more prominent when the samples were compared in terms of reflow duration. It is believed that as reflow duration extended, more Ni diffused out from Ni-P layer to form IMCs [9], [29]. This resulted in the thinning of 0.5  $\mu\text{m}$  Ni-P plating, causing a Mode 2 or 3 failure (at the IMC/Ni interfacial fracture).

Mode 2 and 3 failures either became less frequent or disappeared with thicker Ni-P plating. For C194 samples, Mode 2 became less frequent and Mode 3 disappeared at 4.5  $\mu\text{m}$  Ni-P thickness. On the other hand, EFTECH-64 only showed Mode 1 failure at 4.5  $\mu\text{m}$  Ni-P plated samples. It is believed a thicker Ni-P plating slowed down the IMC's built up and void formation, thus reducing or eliminating the occurrence of Mode 2 and 3 failures in the C194 and EFTECH-64 samples.

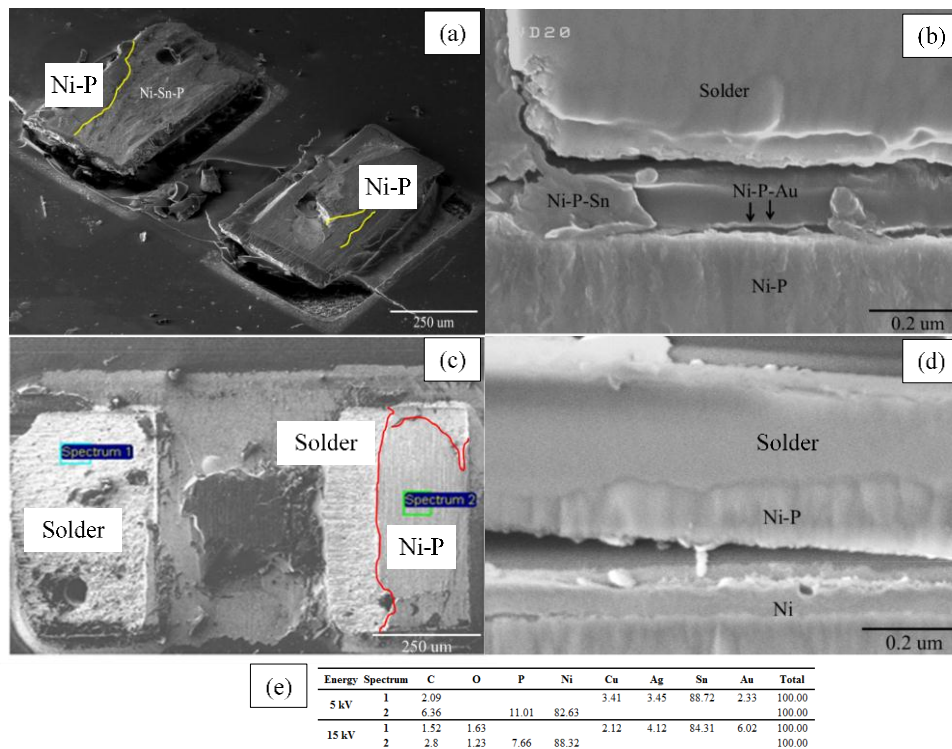


**Figure 10.** SEM images of PCB side fracture surfaces and their corresponding cross-section after shear test on soldered 0.5  $\mu\text{m}$  Ni-P plated samples, reflowed at 240°C for 10 min. C194 sample of (a) shows predominant Mode 2 failure, EFTECH-64 of (c) shows predominant Mode 1 failure. Their respective cross-sectional views are shown in (b) and (d). EDX results of Mode 1 (labeled as 'spectrum 1') and Mode 3 (labeled as 'spectrum 2') in (c) are shown as tabulated elemental concentration data in (e)

Figure 10 illustrates fracture surfaces of the PCB side after the shear test of the solder joint of C194 and EFTECH-64 samples. The two rectangular fracture surfaces corresponded to the solder contact areas of a TSLP unit. Figure 10(a) shows that the C194 displayed a predominant Mode 2 failure area where the major fracture surface was Ni-Sn-P IMC, with smaller Ni-P fracture surface was displayed. The observed chemical compositions of Ni, P and Sn in IMC verified the

formation of Ni-Sn-P IMC, consistent with previous findings [9], [28]. The brittle IMC failure resulted in crack formations on the Ni-P/Ni-Sn-P interface, as shown in Figure 10(b).

Figure 10(c) shows that Mode 1 failure area covered most of the fracture surface with a smaller fracture surface of Ni-P. Mode 1 exhibited the presence of Ag and Sn elements from the Sn-Ag solder. In addition, small amounts of Cu and Au

were detected, originated from the PCB's Cu interconnect and the sputter coating for SEM imaging. A smoother Mode 3 region in Figure 10(c) and (d) showed Ni-P plating remnant that matched with the N:P composition (i.e. 92 wt% Ni-8 wt% P) of Ni-P plating prior to the soldering process. Figure 8(e) shows Ni:P weight ratio of 88:12 and 92:8 were detected at 5 kV and 15 kV EDX settings respectively. We suspect the interaction volume difference contributed to the ratio difference.

## CONCLUSION

We have shown that there is a remarkably strong effect of Thin Small Leadless Packages (TSLP) pad's surface roughness on shear strength and the failure mode of the TSLP's solder joint. Based on the interaction profile analysis of four dominant etching factors, we demonstrated the predominant role of leadframe materials on the surface roughness ( $R_a$ ) of post-etched TSLP's pad. The investigation went further by demonstrating the establishment of the effect of the TSLP pad's  $R_a$  on the Ni-P plating's  $R_a$  and the subsequent solder joint strength, as well as the corresponding failure modes under different Ni-P thicknesses and reflow conditions. The important conclusions observed are as follows:

- Shear strength and strength variation of the solder jointed Ni-P plated TSLP's pad increased with the increase of Ni-P thickness.
- Shear strength variation of C194 was larger than the EFTECH-64. However, both samples show low significant difference in terms of shear strength at a similar Ni-P thickness.
- Most of the shear test samples' failures occurred at the solder region (Mode 1), with a small fraction of the failures occurring at the intermetallic compound (Mode 2). C194 showed higher percentage of Mode 2.
- Failure at the pad/Ni-P interface (Mode 3) of C194 samples was observed after being reflowed at a temperature of 240°C for 10 min.
- $R_a$  decreased with a thicker Ni-P, thus improving the Sn-Ag solder wettability and reducing Mode 2 and 3 failures for both the C194 and EFTECH-64 samples.
- Mode 2 and 3 failures were eliminated from the solder jointed samples when higher reflow temperature and extended reflow duration were used. This was due to the increase of interdiffusion process at a higher reflow temperature (260°C), strengthened the IMC layer.

Although Mode 1 failure occurrence was the highest in soldered jointed samples, the related failure analysis was not widely reported. Thus, we recommend further studies on its root cause by careful SEM-EDX line profiling to verify the relationship between shear strength, failure mode frequency, Ni-P thickness and the pad's roughness.

## ACKNOWLEDGEMENTS

The authors gratefully acknowledge the management support of the Infineon Technologies Sdn. Bhd (Malaysia), Melaka, as well as technical assistance from Universiti Teknikal Malaysia Melaka. Special thanks to Kim-Swee Goh, Mei-Qi Tay, Muhammad Afiq and Kian-Pin Queck from Infineon Technologies for their assistance in sample preparation and characterization.

## REFERENCES

- [1] P. Klaus, B. Gottfried, W. Maciej, *Assembly and Packaging Enabling System Integration*, Proc. International Symposium on Microelectronics, Orlando, 2013, pp. 000171-000176.
- [2] H. Gwee, K. Ng, *A Sample Preparation on Decapsulation Methodology for Effective Failure Analysis on Thin Small Leadless (TSLP) Flip Chip Package with Copper Pillar (CuP) Bump Interconnect Technology*, Proc. ISTFA 2014: Conference Proceedings from the 40th International Symposium for Testing and Failure Analysis, ASM International: Houston, 2014, pp. 100-104.
- [3] M. S. Lim, T. K. Gan, C. W. Wong, *Challenges and countermeasure of strip form reflow screening process for flip chip QFN and module package*, Proc. 17th IEEE Electronics Packaging and Technology Conference (EPTC 2015), 2015, pp. 1-5.
- [4] H. Theuss, *Chip package including a microphone structure and a method of manufacturing the same*, US20140203380 A1, 2016.
- [5] B. S. Lee, C. V. Tan, *Semiconductor device having multiple chips mounted to a carrier*, US9263421 B2, 2016.
- [6] M. T. Ong, T. H. Lim, K. C. Goh, *Bump package and methods of formation thereof*, US9373609 B2, 2016.
- [7] M. Engl, *Package Characterization Techniques and Evaluation of a Plastic Package for mm-Wave Applications*, Dipl.-Ing. Dissertation, University of Erlangen-Nurnberg, 2006.
- [8] E. Suhir, R. Ghaffarian, S. Yi, Reliability physics behind the QFN state of stress, *Journal of Material Science: Materials in Electronic*, Vol. 28, pp. 1-12, 2016.
- [9] A. Kumar, Z. Chen, Effect of Ni-P Thickness on the Tensile Strength of Cu/Electroless Ni-P/Sn-3.5 Ag Solder Joint, Proc. IEEE Transactions on Components and Packaging Technologies, Vol. 29, pp. 886-892, 2006.
- [10] C. A. Loto, Electroless Nickel Plating – A Review, *Silicon*, Vol. 8, n. 2, pp. 177-186, 2016.
- [11] Z. Huber, J. Wojewoda-Budka, A. Wierzbicka-Miernik, A. Sypien, M. Szczerba, P. Zieba, Influence

- of phosphorous content on microstructure development at the Ni-P Plating/SAC interface, *Electronics Materials Letter*, Vol. 12, n. 1, pp. 178-185, 2016.
- [12] C. G. Ong, K. T. Lau, M. Zaimi, M. Afiq, K. P. Queck, *Effect of electroless Ni-P thickness on EFTECH 64-Ni, EFTECH 64-Cu and C194-Ni bump*, Proc. 11th International Microsystems, Packaging, Assembly and Circuits Technology Conference (IMPACT 2016), pp. 319-322, 2016.
- [13] G. O. Mallory, J. B. Hajdu, *Electroless plating: fundamentals and applications* (William Andrew, 1990).
- [14] P. Sahoo, S. K. Das, Tribology of electroless nickel coatings—a review, *Materials Design*, Vol. 32, n. 4, pp. 1760-1775, 2011.
- [15] C. Lee, Corrosion and wear-corrosion resistance properties of electroless Ni-P coatings on GFRP composite in wind turbine blades, *Surface and Coatings Technology*, Vol. 202, n. 19, pp. 4868-4874, 2008.
- [16] Z. Liu, W. Gao, Electroless nickel plating on AZ91 Mg alloy substrate, *Surface and Coatings Technology*, Vol. 200, n. 16, pp. 5087-5093, 2006.
- [17] T. S. Choi, D. W. Hess, Chemical etching and patterning of copper, silver, and gold films at low temperatures, *ECS Journal of Solid State Science Technology*, Vol. 4, n. 1, pp. N3084-N3093, 2005.
- [18] O. Cakir, Copper etching with cupric chloride and regeneration of waste etchant, *Journal of Materials Processing Technology*, Vol. 175, n. 1, pp. 63-68, 2006.
- [19] M. Yu, X. Zeng, Q. Song, L. Liu, J. Li, Examining regeneration technologies for etching solutions: a critical analysis of the characteristics and potentials, *Journal of Cleaner Production*, Vol. 113, pp. 973-980, 2016.
- [20] O. Cakir, *Photochemical machining of brass with cupric chloride etchants*, Ph.D. Thesis, Cranfield University, 1996.
- [21] O. Cakir, H. Temel, M. Kiyak, Chemical etching of Cu-ETP copper, *Journal of Materials Processing Technology*, Vol. 162, pp. 275-279, 2005.
- [22] O. Cakir, Review of etchants for copper and its alloys in wet etching processes, *Key Engineering Materials*, Vol. 364, pp. 460-465, 2008.
- [23] A. Anoop Prakash, J. G. Jency, M. C. Mathew, *A review of various wet etching techniques used in micro fabrication for real estate consumption*, Proc. Int. Conf. Innovation in Intelligent Instrumentation, Optimization and Signal Processing, Coimbatore, 2013, pp. 26-31.
- [24] P. Pal, A. Ashok, S. Halder, Y. Xing, K. Sato, Anisotropic etching in low-concentration KOH: effects of surfactant concentration, *Micro & Nano Letter*, Vol. 10, n. 4, pp. 224-228, 2015.
- [25] NACE International, *Chapter 1, Corrosion Control in the Refining Industry* (NACE International, 2010).
- [26] W. R. Osório, A. Garcia, Interrelation of wettability–microstructure–tensile strength of lead-free Sn–Ag and Sn–Bi solder alloys, *Science Technology of Welding and Joining*, Vol. 21, n. 6, pp. 429-437, 2016.
- [27] P. Yao, X. Li, X. Liang, B. Yu, Investigation of soldering process and interfacial microstructure evolution for the formation of full Cu<sub>3</sub>Sn joints in electronic packaging, *Materials Sciences in Semiconductor Process*, Vol. 58, pp. 39-50, 2017.
- [28] Mona, A. Kumar, Z. Chen, *Influence of Phosphorus Content on the Interfacial Microstructure Between Sn-3.5Ag Solder and Electroless Ni-P Metallization on Cu Substrate*, Proc. IEEE Transactions on Advanced Packaging, 2007, Vol. 30, n. 1, pp. 68-72.
- [29] C. K. Chung, Y. Chen, W. Chen, C. Kao, Origin and evolution of voids in electroless Ni during soldering reaction, *Acta Materials*, Vol. 60, n. 11, pp. 4586-4593, 2012.
- [30] Technofil, Company Profile. <http://www.tecnofil.com.pe/images/upload/paginaweb/archivo/13/Tecnofil%202016.pdf>, Accessed date: 14 May 2017
- [31] Furukawa Electric Group, High Performance Copper Alloy for Leadframe: EFTEC-64T EFTEC-64T-C. [https://www.furukawa.co.jp/english/tukuru/pdf/eftec64t\\_e.pdf](https://www.furukawa.co.jp/english/tukuru/pdf/eftec64t_e.pdf), Accessed date: 13 May 2017.
- [32] C. G. Ong, K. T. Lau, M. Zaimi, K. S. Goh, M. Q. Tay, *Effect of Cu based complexes on EFTECH 64 and C194 Cu alloy*, Proc. 2016 IEEE 37th International Electronics Manufacturing Technology (IEMT) & 18th Electronics Materials and Packaging (EMAP), 2016, pp. 1-4.
- [33] IPC, 2.2.17A Surface Roughness, In *IPC-TM-650 Test Method Manual* (2001).
- [34] IPC, Amendment 1 Specification for Electroless Nickel/Immersion Gold (ENIG) Plating for Printed Circuit Boards In *IPC 4552* (2012).
- [35] IPC, 2.4.1 Adhesion, Tape Testing, In *IPC-TM-650 Test Method Manual* (2004).
- [36] IPC, Peak reflow temperatures for a lead-free soldering operation, In *JEDEC J-STD-020D* (2008).
- [37] J. E. Charles Jr, *Etching control device, 3,553,052*, 1979.
- [38] M. S. Silberberg, *Chemistry: The Molecular Nature of Matter and Change* (5th edition, McGraw Hill, New York, 2008).

- [39] K. Feng, N. Kapadia, B. Jobson, S. Castaldi, *Cupric Chloride-Hydrochloric Acid Microetch Roughening Process and its Applications*, Proc. 10<sup>th</sup> IEEE Electronics Packaging Technology Conference, 2008, pp 103-108.
- [40] L. Vivet, A. L. Joudrier, K. L. Tan, J. M. Morelle, A. Etcheberry, L. Chalumeau, Influence of nickel–phosphorus surface roughness on wettability and pores formation in solder joints for high power electronic applications, *Applied Surface Science*, Vol. 287, pp. 13-21, 2013.
- [41] C. Liu, D. A. Hutt, D. Li, P. P. Conway, *Effect of Microstructural Characteristics of Electroless Nickel Metallisation on Solderability to Pb-Free Solder Alloys*, Proc. ASME 2005 Pacific Rim Technical Conference and Exhibition on Integration and Packaging of MEMS, NEMS, and Electronic Systems collocated with the ASME 2005 Heat Transfer Summer Conference, 2005, pp. 1819-1825.